

This discussion paper is/has been under review for the journal Atmospheric Measurement Techniques (AMT). Please refer to the corresponding final paper in AMT if available.

Characterization and first results of an ice nucleating particle measurement system based on counterflow virtual impactor technique

L. P. Schenk¹, S. Mertes¹, U. Kästner¹, F. Frank², B. Nillius^{2,*}, U. Bundke^{2,**},
D. Rose², S. Schmidt³, J. Schneider³, A. Worringer⁴, K. Kandler⁴,
N. Bukowiecki⁵, M. Ebert⁴, J. Curtius², and F. Stratmann¹

¹Leibniz Institute for Tropospheric Research, Leipzig, Germany

²Institute for Atmospheric and Environmental Sciences, Goethe University of Frankfurt am Main, Frankfurt am Main, Germany

³Max Planck Institute for Chemistry, Particle Chemistry Department, Mainz, Germany

⁴Technical University of Darmstadt, Institute of Applied Geosciences, Darmstadt, Germany

⁵Laboratory of Atmospheric Chemistry, Paul Scherrer Institute (PSI), Villigen, Switzerland

* now at: Max Planck Institute for Chemistry, Particle Chemistry Department, Mainz, Germany

** now at: Jülich Research Center, Institute of Energy and Climate Research, Troposphere (IEK-8), Jülich, Germany

10585

Received: 11 September 2014 – Accepted: 26 September 2014 – Published: 21 October 2014

Correspondence to: L. P. Schenk (schenk@tropos.de)

Published by Copernicus Publications on behalf of the European Geosciences Union.

10586

Abstract

A specific instrument combination was developed to achieve a better microphysical and chemical characterization of atmospheric aerosol particles that have the potential to act as ice nucleating particles (INP). For this purpose a pumped counterflow virtual impactor system called IN-PCVI was set up and characterized to separate ice particles that had been activated on INP in the Fast Ice Nucleus Chamber (FINCH) from interstitial, non-activated particles. This coupled setup consisting of FINCH (ice particle activation and counting), IN-PCVI (INP separation and preparation), and further aerosol instrumentation (INP characterization) had been developed for the application in field experiments. The separated INP were characterized on-line with regard to their total number concentration, number size distribution and chemical composition, especially with the Aircraft-based Laser Ablation Aerosol Mass Spectrometer ALABAMA. Moreover, impactor samples for electron microscopy were taken. Due to the coupling the IN-PCVI had to be operated with different flow settings than known from literature, which required a further characterization of its cut-off-behavior. Taking the changed cut-off-behavior into account, the INP number concentration measured by the IN-PCVI system was in good agreement with the one detected by the FINCH optics for water saturation ratios up to 1.01 (ice saturation ratios between 1.21–1.34 and temperatures between -18 and -26 °C). First field results of INP properties are presented which were gained during the INUIT-JFJ/CLACE 2013 campaign at the high altitude research station Jungfrauoch in the Bernese Alps, Switzerland (3580 m a.s.l.).

1 Introduction

Ice crystals in clouds influence precipitation and the microphysical and thus the radiative properties of clouds. They play an important role for the cloud lifetime, the interactions of clouds with solar radiation, cloud electricity and cloud dynamics. Mixed-phase clouds consisting of supercooled droplets and ice particles exist at altitudes

10587

where temperatures warmer than -38 °C occur. In such clouds, ice can only be formed heterogeneously, due to the presence of so-called ice nucleating particles (INP) (Vali et al., 2014; DeMott et al., 2011; Pruppacher and Klett, 1997). Known pathways of heterogeneous ice formation are deposition nucleation and condensation, immersion and contact freezing. Field data and modeling studies indicate for many situations that liquid water droplets are a prerequisite for ice formation (Murray et al., 2012; Westbrook and Illingworth, 2011; de Boer et al., 2011; Ansmann et al., 2009). This suggests an important role of immersion and contact freezing processes in atmospheric ice formation. But also sub-saturated nucleation processes (Sassen and Khvorostyanov, 2008) (e.g. deposition nucleation) were found to be an active freezing mechanism under atmospheric conditions. However, the relative importance of the different pathways is not well known at present.

Many species have been identified to act as INP, e.g. mineral dust (e.g., illite, montmorillonite, kaolinite, feldspar), primary biological particles (PBAP), soot, and glassy organics. In laboratory experiments many of these models substances were investigated and their ice forming efficiencies (nucleation temperatures and rates) have been quantified and parameterized (e.g. Murray et al., 2010; Hoose and Moehler, 2012; Atkinson et al., 2013; Wex et al., 2014). However, the type of ambient aerosol particles acting as INP, the importance of their size and the influence of anthropogenically emitted aerosol particles are not well understood. There is still a lack of field measurements concerning the in-situ physio-chemical characterization of atmospheric INP.

In 2011 the Ice Nuclei Research Unit (INUIT) was established with the objective to achieve a more detailed understanding of heterogeneous ice forming processes. The central objective of INUIT is to obtain a better knowledge of ambient aerosol particles serving as INP. Therefore, an ice nucleus counter was connected by means of the counterflow virtual impactor (CVI) technique to online mass spectrometry, and other aerosol measurement techniques, similar to the coupling that had been originally presented by Cziczo et al. (2003) and some years later by Corbin et al. (2012). Corbin et al. (2012) presented measurements from a field study in downtown Toronto (SPORT

10588

detector consists of a 405 nm laser, which stimulates the particles to fluoresce as well. In this study the outlet of the BIO-IN-OPC was directly connected to the IN-PCVI.

After several hours of operation the measurements with FINCH are interrupted for a short heating period to melt the ice that had built up in the inlet and thus resulted in a reduced or plugged flow. After every heating period the saturation ratio inside FINCH is automatically re-established to the set value, which can take up to an hour. During operation S_{ice_F} is adjusted continuously as a consequence of changing ambient temperature and relative humidity.

2.3 Aircraft-based laser ablation aerosol mass spectrometer (ALABAMA)

ALABAMA is a single particle laser ablation instrument to detect the chemical composition, mixing state and size of aerosol particles in a range from 150–900 nm (Brands et al., 2011). It was built and characterized at the Max Planck Institute for Chemistry (MPIC) Mainz. The particles are detected and sized by two continuous lasers at a wavelength of 405 nm (InGaN Blu-Ray laser). Thereafter, a 266 nm wavelength pulsed Nd-YAG-laser is used to evaporate the aerosol particles and ionize the components. A bipolar, Z-shaped time-of-flight mass spectrometer (Tofwerk) generally detects positive and negative ions. During the INUIT-JFJ/CLACE 2013 campaign only positive ions were detected due to technical issues. It is used to measure the chemical composition of FINCH-detected INP, which are separated, sampled and released by the IN-PCVI.

2.4 Microphysical aerosol instrumentation

For a microphysical characterization of the INP a condensation particle counter (CPC TSI 3010) and an aerodynamic particle sizer (APS TSI 3321) were connected downstream the IN-PCVI. The CPC measures the number concentration of particles that are larger than 0.01 μm in diameter.

10593

The APS measures the aerodynamic number size distribution of aerosol particles in the size range between 0.5 and 20 μm . The sizing is done by a time-of-flight measurement between two laser beams. The IN-PCVI in combination with CPC and APS are called IN-PCVI system in the following.

2.5 Scanning electron microscopy (SEM)

Ice-nucleating particles were collected downstream the IN-PCVI by a two-stage impactor system (50 % cut-off aerodynamic diameters 1.0 and 0.1 μm , respectively) and were analyzed offline by scanning electron microscopy and energy-dispersive X-ray fluorescence (EDX). Particles were collected on transmission electron microscopy grids and elemental boron. The samples were analyzed in a scanning electron microscope (FEI Quanta 200 FEG, FEI, Eindhoven, the Netherlands) with attached energy-dispersive X-ray fluorescence microanalysis (EDX, EDAX, Tilburg, the Netherlands) to characterize the particles with regard to their chemical composition, morphology, size, internal mixing state and electron beam stability (volatility). Based on criteria of chemical composition, morphology mixing state and beam stability, particles were sorted into ten singular classes (carbonaceous, sulfate and other secondary aerosol, soot, sea-salt, Ca-rich, metal oxide, silicate, Pb-bearing, droplets, and other particles). For details on the particle classes, the reader is referred to Worringer et al. (2014). Due to their low abundance, in the present work sea-salt and Pb-bearing particles are summarized with all other unclassified particles into the so-called “other” class.

2.6 Test measurements in the laboratory

Prior to field operation, the volume flow management of the combination of FINCH, the IN-PCVI and several aerosol particle instruments was set up and tested during two technical laboratory campaigns in Frankfurt and Leipzig. Since each component has its own standalone flow system, the main concern was to adapt and couple the flows and to ensure a smooth and efficient transition of the sample from one component

10594

to the following one. As a main result of these tests, the FINCH closed loop had to be switched off and the FINCH aerosol flow had to be directly controlled by the IN-PCVI pump flow. This led to stable pressure conditions inside the coupled FINCH + IN-PCVI flow system. Additionally, it was found that changes in the IN-PCVI – FINCH flows caused fluctuations in the supersaturation of FINCH, which sometimes resulted in a frozen inlet and thus blocking of the growth chamber. Therefore, the FINCH – IN-PCVI flows were kept constant during single measurement runs.

2.7 Atmospheric measurements at the high Alpine research station Jungfraujoch

The combination of INP activation and detection (FINCH), separation/preparation (IN-PCVI), and characterization (aerosol instrumentation) was deployed in January/February 2013 during the INUIT-JFJ/CLACE-2013 joint measurement field campaign (Schneider et al., 2014) at the Sphinx Laboratory of the high Alpine research station Jungfraujoch (JFJ, Bernese Alps, Switzerland, 3580 m a.s.l.). The combination of FINCH, IN-PCVI, and aerosol instruments was deployed at this site to sample aerosol particles inside mixed-phase or, sometimes, even entirely glaciated clouds, where supercooled drops and small ice particles were evaporated during collection by heated total aerosol inlet (operated by Paul Scherrer Institute, Villigen; Weingartner et al., 1999). Also ambient background aerosol particles, which are present during cloud free time periods, are sampled at these altitude that are realistic for the mixed-phase cloud formation at mid latitudes.

10595

3 Results

3.1 Proof of principle for the FINCH + IN-PCVI coupling

The main focus of this work was to verify the feasibility of the FINCH + IN-PCVI coupling for the physical and chemical characterization of atmospheric INP by different aerosol sensors attached to the IN-PCVI.

A stability criterion of the adjusted ice saturation ratio inside FINCH needed to be specified to ensure the data analysis under constant measurement conditions. Fluctuations in the FINCH saturation ratio may lead to different conditions under which freezing occurs and thus to differences in the final sizes to which the ice particles grow. Therefore, only measurement periods in which the ice saturation ratio varied by less than 1 % (relatively) within 300 s were used for further analysis. This criterion is somewhat arbitrary, but appeared to effectively eliminate the poorly defined activation periods while leaving sufficient amount of data points for the proof-of-principle study.

During the INUIT-JFJ/CLACE-2013 campaign the complete coupled system of FINCH, IN-PCVI and aerosol instruments was connected to the heated total aerosol inlet sampling line to investigate the ice activation ability of ambient aerosol particles and during cloud periods also of cloud ice particle residuals and cloud droplet residuals. For this purpose FINCH was operated in the temperature range between -18 and -26 °C and at ice saturation ratios between 1.05 and 1.5. Figure 6 shows the $T_F - S_{ice_F}$ pairs (10 min averages) from the campaign that remain after applying the stability criterion. Moreover, the corresponding lines of the calculated water saturation ratio (0.90 to 1.25 in 0.05 steps) are indicated. The majority of the 10 min periods used in the following discussion are located in the water supersaturated region ($S_{wat_F} > 1.0$) when immersion freezing is the dominant heterogeneous ice nucleation mechanism inside FINCH. Only a few data points are below $S_{wat_F} = 1.0$ when ice activation in FINCH is limited to deposition nucleation and immersion freezing in highly concentrated solution droplets (Wex et al., 2014) only. Figure 7 shows a log-log scatterplot of the number concentration of ice nucleating particles measured by the FINCH optics (N_{INP_FINCH}) and

10596

measured by the IN-PCVI CPC ($N_{\text{INP,IN-PCVI}}$, same 10 min averages). The data points are subdivided into 3 classes with regard to the prevailing FINCH water saturation ratio:

$S_{\text{wat}_F} < 1.0$ (squares), $1.0 < S_{\text{wat}_F} < 1.1$ (circles) and $1.1 < S_{\text{wat}_F} < 1.2$ (crosses).

5 The 1 : 1 line indicated in Fig. 7 shows that there exists a very close correlation between $N_{\text{INP,FINCH}}$ and $N_{\text{INP,IN-PCVI}}$ for $S_{\text{wat}_F} < 1.0$ (squares), which implies that the residue of each ice particle grown in FINCH is transferred with high efficiency through the IN-PCVI and all other particles exiting FINCH (supercooled droplets, unactivated particles) are diverted into the F_{PF} of the IN-PCVI. With increasing water saturation ratio, however,
 10 $N_{\text{INP,IN-PCVI}}$ concentration exceeds $N_{\text{INP,FINCH}}$. Since it is not likely that more ice nucleating particles exist after the IN-PCVI than there were ice particles counted after FINCH, the most probable explanation is that some liquid supercooled droplets that are formed in FINCH reach the same size as the ice particles at higher saturation. Thus, they cannot be pre-segregated by the IN-PCVI and become erroneously counted and sampled
 15 as INP. In order to estimate the magnitude of this effect, power regressions (with an exponent equal 1) were calculated for each class and plotted in Fig. 7. These indicate contribution of large droplet residuals 0, 45, and 63% for the intended INP sampling with respect to the three S_{wat_F} classes.

Table 2 gives a more detailed verification of the droplet contamination effect. Again
 20 power regressions are derived from the $N_{\text{INP,FINCH}}$ to $N_{\text{INP,IN-PCVI}}$ relationship but now separately for a S_{wat_F} increment of 0.01. The desired regression close to 1 is only achieved for $S_{\text{wat}_F} \leq 1.01$, which denotes an ice saturation between 1.21 and 1.3 for the adjusted temperatures. However, the uncertainty of the regression slope includes 1 still for a $S_{\text{wat}_F} \leq 1.06$ ($1.21 < S_{\text{ice}_F} < 1.34$). Accepting a ratio of one drop residual out of
 25 three INP_{IN-PCVI} would allow to take into account all measurements up to $S_{\text{wat}_F} \leq 1.08$ ($1.21 < S_{\text{ice}_F} < 1.34$). For all INP results obtained by the coupled system these limitations and uncertainties have to be taken into account.

10597

3.2 First measurements of INP properties

Having proven the feasibility and discussed the operational limitations of the FINCH + IN-PCVI coupling, now first exemplary results of INP properties obtained with this experimental setup during the INUIT-JFJ/CLACE-2013 campaign are presented. Identical
 5 to the experimental setup described in Sect. 3.1 ambient particles as well as residues of supercooled drops or ice particles in the presence of clouds were sampled by the heated total aerosol inlet, to which the combination of FINCH, IN-PCVI, and aerosol sensors was connected to. During all measurements at the JFJ the IN-PCVI cut-off diameter was adjusted in the characterized range, which is shown in Fig. 5a–c. Figure 8
 10 shows an INP time series from a 4 h case study on 9 February 2013. The data points are again 10 min mean values and meet the above described criterion of the FINCH saturation ratio varying less than 1% in 300 s. Within this period T_F was adjusted in a range from -21 to -23.5 °C and S_{ice_F} to ~ 1.1 , respectively. Thus, FINCH was operated at water sub-saturated conditions, i.e. deposition nucleation and/or immersion
 15 freezing of highly concentrated solutions are the prevailing heterogeneous nucleation mechanisms inside FINCH. Consistent with the findings in Sect. 3.1, the FINCH and IN-PCVI INP concentrations agree very well in this case study increasing from 5 to 25 L^{-1} . The reason for the increase of the INP concentration by a factor of 5 within 3 h is not clear, but a decisive change in the air mass can be ruled out.

Another measure for the INP number concentration is inferred from integrating the
 20 INP number size distribution measured by the APS (Fig. 8). The lower size detection limit of the APS is $0.55 \mu\text{m}$, i.e., the APS $N_{\text{INP,IN-PCVI}}$ refers to all INP_{IN-PCVI} larger than this diameter. The variation of the concentration of these large INP in time shows the same increasing trend but on a substantially lower level between 0 to 4 L^{-1} , which is a factor of 7 below the values of the total INP concentration. Hence, it can be concluded that only 13% of the sampled INP are larger than $0.55 \mu\text{m}$ and the majority of the INP (87%) are smaller for the situation encountered in this case study. Tests of
 25 the reduced counting efficiency in the lower APS channels (555–700 nm) showed only

10598

- spectrometry of ice nuclei, *Aerosol Sci. Tech.*, 37, 460–470, doi:10.1080/02786820300976, 2003. 10588
- de Boer, G., Morrison, H., Shupe, M. D., and Hildner, R.: Evidence of liquid dependent ice nucleation in high-latitude stratiform clouds from surface remote sensors, *Geophys. Res. Lett.*, 38, L01803, doi:10.1029/2010GL046016, 2011. 10588
- 5 DeMott, P. J., Prenni, A. J., Liu, X., Kreidenweis, S. M., Petters, M. D., Twohy, C. H., Richardson, M. S., Eidhammer, T., and Rogers, D. C.: Predicting global atmospheric ice nuclei distributions and their impacts on climate, *P. Natl. Acad. Sci. USA*, 107, 11217–11222, doi:10.1073/pnas.0910818107, 2010. 10599
- 10 DeMott, P. J., Möhler, O., Stetzer, O., Vali, G., Levin, Z., Petters, M. D., Murakami, M., Leisner, T., Bundke, U., Klein, H., Kanji, Z. A., Cotton, R., Jones, H., Benz, S., Brinkmann, M., Rzesanke, D., Saathoff, H., Nicolet, M., Saito, A., Nillius, B., Bingemer, H., Abbatt, J., Ardon, K., Ganor, E., Georgakopoulos, D. G., and Saunders, C.: Resurgence in ice nuclei measurement research, *B. Am. Meteorol. Soc.*, 92, 1623–1635, doi:10.1175/2011BAMS3119.1, 2011. 10588
- 15 Eidhammer, T., DeMott, P. J., and Kreidenweis, S. M.: A comparison of heterogeneous ice nucleation parameterizations using a parcel model framework, *J. Geophys. Res.-Atmos.*, 114, D06202, doi:10.1029/2008JD011095, 2009. 10599
- Hiranuma, N., Kohn, M., Pekour, M. S., Nelson, D. A., Shilling, J. E., and Cziczo, D. J.: Droplet activation, separation, and compositional analysis: laboratory studies and atmospheric measurements, *Atmos. Meas. Tech.*, 4, 2333–2343, doi:10.5194/amt-4-2333-2011, 2011. 10589
- 20 Hoose, C. and Möhler, O.: Heterogeneous ice nucleation on atmospheric aerosols: a review of results from laboratory experiments, *Atmos. Chem. Phys.*, 12, 9817–9854, doi:10.5194/acp-12-9817-2012, 2012. 10588
- 25 Hu, Y., Yang, P., Lin, B., Gibson, G., and Hostetler, C.: Discriminating between spherical and non-spherical scatterers with lidar using circular polarization: a theoretical study, *J. Quant. Spectrosc. Ra.*, 79, 757–764, doi:10.1016/S0022-4073(02)00320-5, 6th International Conference on Electromagnetic and Light Scattering by Nonspherical Particles, Univ. Florida, Gainesville, FL, 4–8 March 2002, 2003. 10592
- 30 Kulkarni, G., Pekour, M., Afchine, A., Murphy, D. M., and Cziczo, D. J.: Comparison of experimental and numerical studies of the performance characteristics of a pumped counterflow virtual impactor, *Aerosol Sci. Tech.*, 45, 382–392, doi:10.1080/02786826.2010.539291, 2011. 10590, 10592, 10612

10603

- Mason, B. J.: *The Physics of Clouds*, Clarendon Press, Oxford, 1971. 10599
- Mertes, S., Verheggen, B., Walter, S., Connolly, P., Ebert, M., Schneider, J., Bower, K. N., Cozic, J., Weinbruch, S., Baltensperger, U., and Weingartner, E.: Counterflow virtual impactor based collection of small ice particles in mixed-phase clouds for the physico-chemical characterization of tropospheric ice nuclei: sampler description and first case study, *Aerosol Sci. Tech.*, 41, 848–864, doi:10.1080/02786820701501881, 2007. 10599
- 5 Murray, B. J., Wilson, T. W., Dobbie, S., Cui, Z., Al-Jumur, S. M. R. K., Moehler, O., Schnaiter, M., Wagner, R., Benz, S., Niemand, M., Saathoff, H., Ebert, V., Wagner, S., and Kaercher, B.: Heterogeneous nucleation of ice particles on glassy aerosols under cirrus conditions, *Nat. Geosci.*, 3, 233–237, doi:10.1038/NGEO817, 2010. 10588
- 10 Murray, B. J., O’Sullivan, D., Atkinson, J. D., and Webb, M. E.: Ice nucleation by particles immersed in supercooled cloud droplets, *Chem. Soc. Rev.*, 41, 6519–6554, doi:10.1039/C2CS35200A, 2012. 10588
- Pruppacher, H. and Klett, J.: *Microphysics of Clouds and Precipitation*, Kluwer, Dordrecht, The Netherlands, ISBN: 0-7923-4211-9, 1997. 10588, 10599
- 15 Rogers, D. C., DeMott, P. J., Kreidenweis, S. M., and Chen, Y.: Measurements of ice nucleating aerosols during SUCCESS, *Geophys. Res. Lett.*, 25, 1383–1386, doi:10.1029/97GL03478, 1998. 10599
- Sassen, K. and Khvorostyanov, V. I.: Cloud effects from boreal forest fire smoke: evidence for ice nucleation from polarization lidar data and cloud model simulations, *Environ. Res. Lett.*, 3, 025006, doi:10.1088/1748-9326/3/2/025006, 2008. 10588
- 20 Slowik, J. G., Cziczo, D. J., and Abbatt, J. P. D.: Analysis of cloud condensation nuclei composition and growth kinetics using a pumped counterflow virtual impactor and aerosol mass spectrometer, *Atmos. Meas. Tech.*, 4, 1677–1688, doi:10.5194/amt-4-1677-2011, 2011. 10589
- 25 Vali, G., DeMott, P., Möhler, O., and Whale, T. F.: Ice nucleation terminology, *Atmos. Chem. Phys. Discuss.*, 14, 22155–22162, doi:10.5194/acpd-14-22155-2014, 2014. 10588
- Weingartner, E., Nyeki, S., and Baltensperger, U.: Seasonal and diurnal variation of aerosol size distributions ($10 < D < 750$ nm) at a high-alpine site (Jungfraujoch 3580 m a.s.l.), *J. Geophys. Res.-Atmos.*, 104, 26809–26820, doi:10.1029/1999JD900170, 1999. 10595
- 30 Westbrook, C. D. and Illingworth, A. J.: Evidence that ice forms primarily in supercooled liquid clouds at temperatures $> -27^\circ\text{C}$, *Geophys. Res. Lett.*, 38, L14808, doi:10.1029/2011GL048021, 2011. 10588

10604

- Wex, H., DeMott, P. J., Tobo, Y., Hartmann, S., Rösch, M., Clauss, T., Tomsche, L., Niedermeier, D., and Stratmann, F.: Kaolinite particles as ice nuclei: learning from the use of different kaolinite samples and different coatings, *Atmos. Chem. Phys.*, 14, 5529–5546, doi:10.5194/acp-14-5529-2014, 2014. 10588, 10596
- 5 Worringer, A., Kandler, K., Benker, N., Dirsch, T., Weinbruch, S., Mertes, S., Schenk, L., Kästner, U., Frank, F., Nillius, B., Bundke, U., Rose, D., Curtius, J., Kupiszewski, P., Weingartner, E., Schneider, J., Schmidt, S., and Ebert, M.: Single-particle characterization of ice-nucleating particles and ice particle residuals sampled by three different techniques, *Atmos. Chem. Phys. Discuss.*, 14, 23027–23073, doi:10.5194/acpd-14-23027-2014, 2014. 10594, 10600
- 10

10605

Table 1. Flow setup of the IN-PCVI (counterflow (F_{CF}), input flow (F_{IF}), sample flow (F_{SF})) resulting in different cut-off-diameters ($D_{p50\%}$).

Run	F_{CF} (L min ⁻¹)	F_{IF} (L min ⁻¹)	F_{SF} (L min ⁻¹)	$D_{p50\%}$ (μm)	
1	3	5	1	5.6	
2	3	5	2	6.5	
3	3	5	3	7.9	
4	2	5	1.3	5.2	
5	2.5	5	1.3	6	
6	3	5	1.3	6.2	
7	3.5	5	1.3	6.5	
8	3	4	1.3	8.4	
9	3	4.5	1.3	7.8	
10	3	5	1.3	6.2	

10606

Table 2. Slope a of the $N_{\text{INP-IN-PCVI}} - N_{\text{INP-IN-PCVI}}$ scatter plot regression depending on the considered water saturation range, the standard deviation (SD) of a , the derived relative droplet contaminations (RDC) and corresponding ice saturation ratios for the investigated temperature range.

S_{wat_F} range	a	SD(a)	RDC (%)	$S_{\text{ice}_F}(-18^\circ\text{C}) - S_{\text{ice}_F}(-26^\circ\text{C})$
≤ 1	0.94	0.05	0	1.2–1.3
≤ 1.01	1.03	0.22	3	1.21–1.31
≤ 1.02	1.12	0.26	12	1.22–1.33
≤ 1.03	1.09	0.22	9	1.24–1.34
≤ 1.04	1.08	0.2	8	1.25–1.35
≤ 1.05	1.13	0.2	13	1.26–1.37
≤ 1.06	1.17	0.18	17	1.27–1.38
≤ 1.07	1.18	0.17	18	1.28–1.39
≤ 1.08	1.24	0.14	24	1.3–1.41
≤ 1.09	1.26	0.13	26	1.31–1.42
≤ 1.1	1.32	0.1	32	1.32–1.43
≤ 1.2	1.53	0.07	53	1.44–1.56

10607

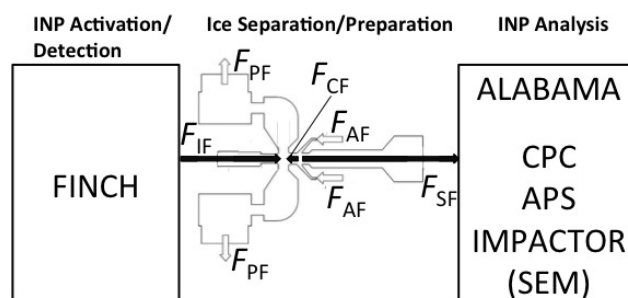


Figure 1. Schematics of the coupled FINCH – IN-PCVI – analysis setup. FINCH activates the INP and counts the grown ice crystals. The IN-PCVI separates these ice particles from non-activated aerosol particles and smaller supercooled droplets, which are also formed inside FINCH. The released INP are transferred to the aerosol sensors for chemical and physical analysis. Flows inside the IN-PCVI are illustrated by arrows and described in the text.

10608

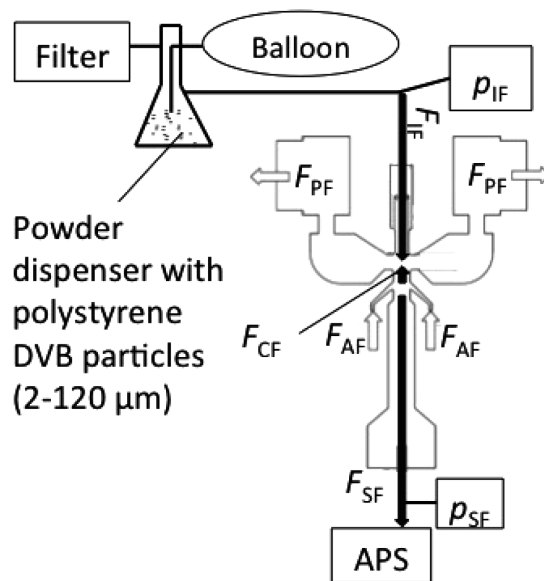


Figure 2. Sketch of the measurement setup for the IN-PCVI $D_{p50\%}$ characterization. A pump bottle is used to disperse polystyrene DVP particles (2–120 μm). The APS of the IN-PCVI system connected downstream of the IN-PCVI measured the reference size distribution (F_{CF} switched off) and the size distribution when the counterflow was switched on. The pressure is measured up- and downstream the IN-PCVI to ensure stable flow conditions (p_{IF} and p_{SF}).

10609

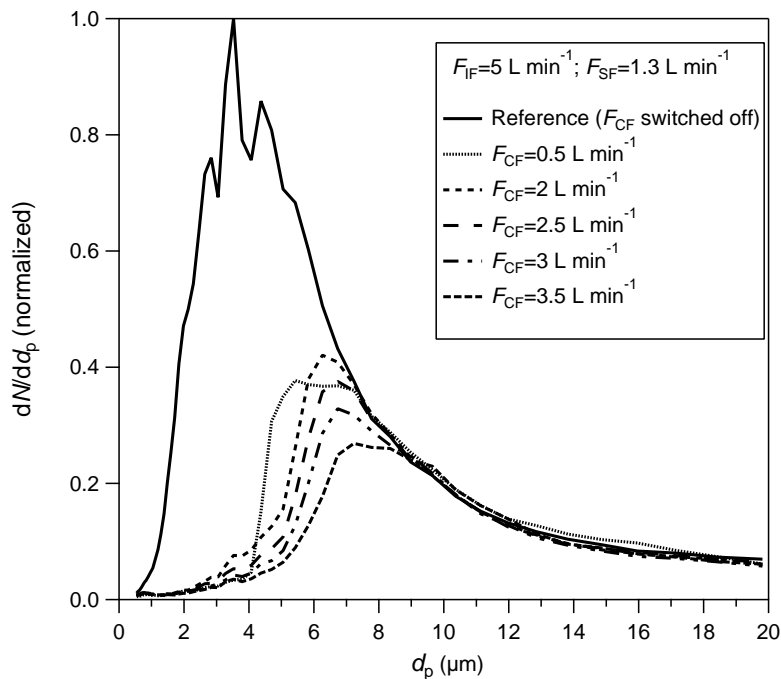


Figure 3. Polystyrene DVB reference number size distribution (solid line) and number size distributions at different counterflows (see legend). All number size distributions were measured by the APS and were normalized to a maximum of 1.

10610

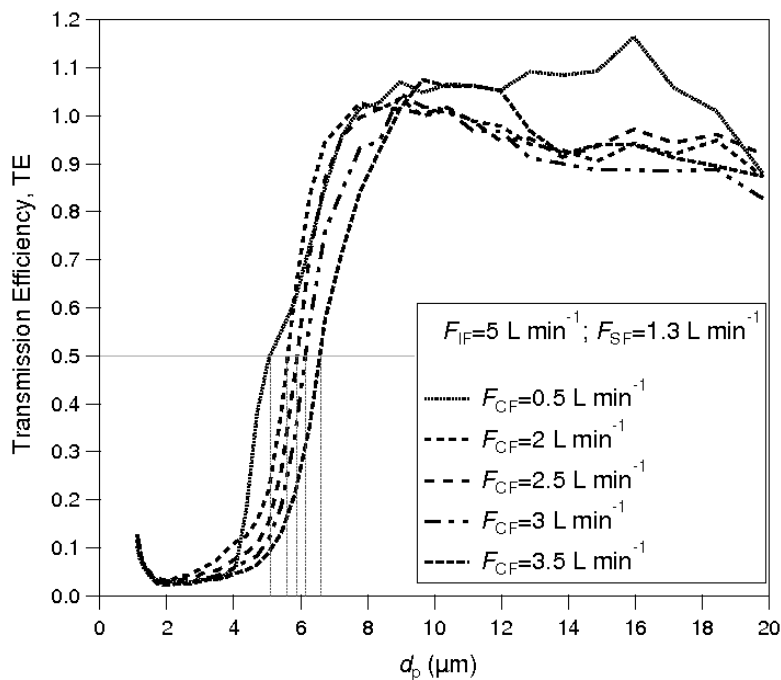


Figure 4. Transmission efficiency of the IN-PCVI derived from the number size distributions shown in Fig. 3. Vertical lines indicate the variation of $D_{p50\%}$ as a function of the counterflow.

10611

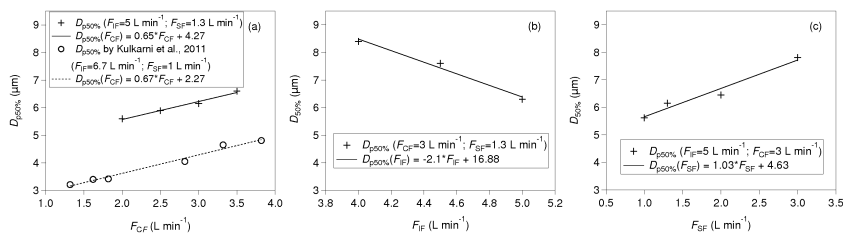


Figure 5. The IN-PCVI cut-off diameter, $D_{p50\%}$ for a changing (a) counterflow F_{CF} , (b) input flow F_{IF} and (c) sample flow F_{SF} . In (a) the variation of the $D_{p50\%}$ with F_{CF} as characterized by Kulkarni et al. (2011) is plotted as circles with a dashed regression line.

10612

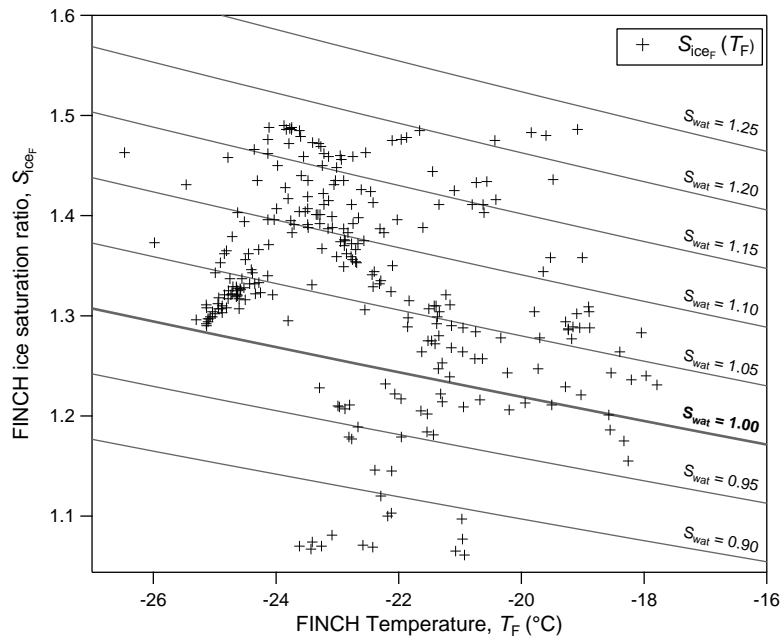


Figure 6. Ice activation conditions in FINCH cover a range of combinations of temperatures (T_F) and ice saturation ratios (S_{iceF}). The majority of measurements was conducted at conditions supersaturated with respect to water (lines of constant S_{watF} are plotted in grey (0.05 steps)).

10613

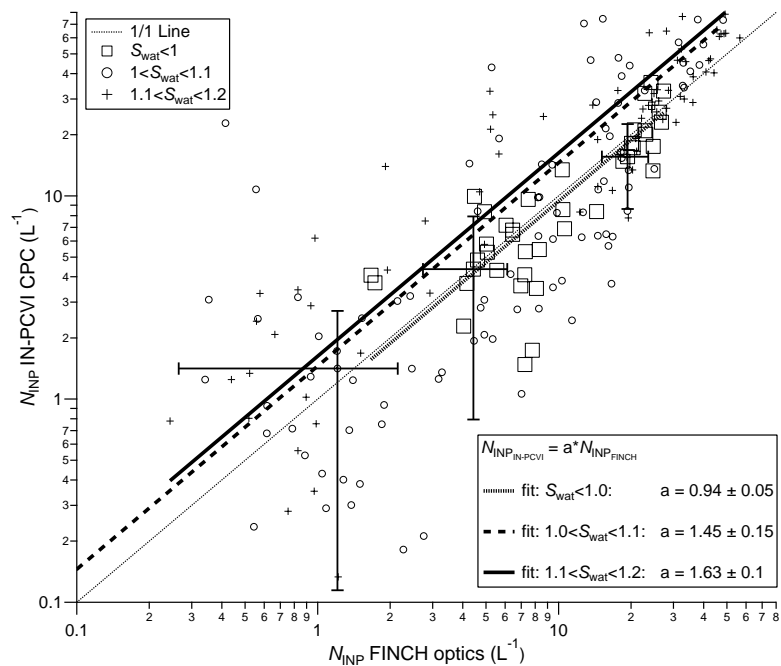


Figure 7. Scatter plot of the INP 10 min averaged number concentrations measured by the FINCH optics and the CPC of the IN-PCVI system, respectively. The concentrations are subdivided into three different water saturation ranges: $S_{watF} < 1.0$ (squares), $1.0 < S_{watF} < 1.1$ (circles) and $1.1 < S_{watF} < 1.2$ (crosses). The power regression curves (exponent equal 1) for these three classes are plotted as lines: $S_{watF} < 1.0$ (dotted line), $1.0 < S_{watF} < 1.1$ (dashed line) and $1.1 < S_{watF} < 1.2$ (solid line). For every number concentration range an example of the standard deviation is indicated by error bars.

10614

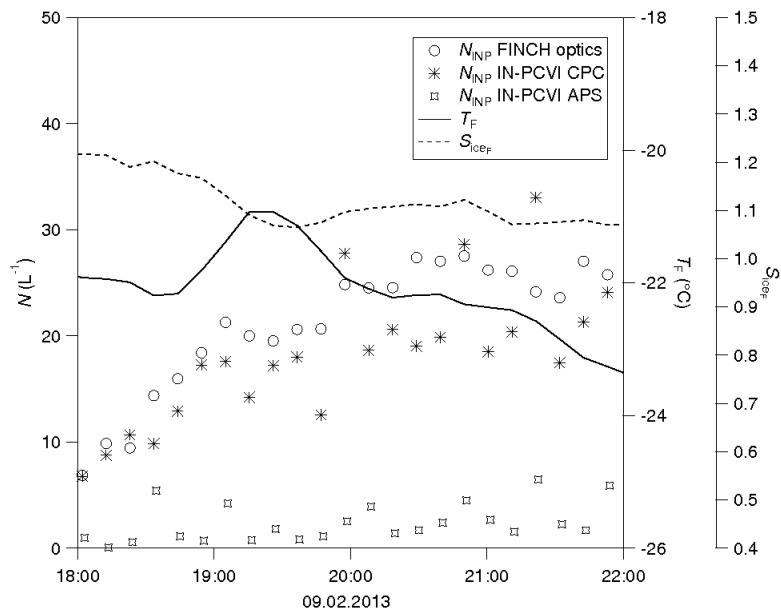


Figure 8. Time series of the INP number concentration (10 min averages) measured by the FINCH optics and by the IN-PCVI system (CPC and APS). The FINCH thermodynamic conditions are plotted as solid (temperature) and dashed (ice saturation) lines on the axes on the right hand side.

10615

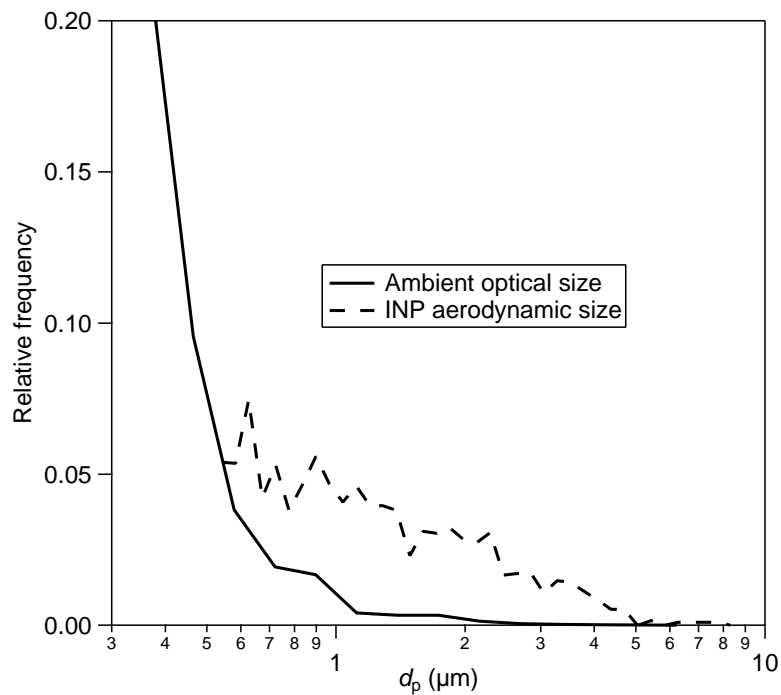


Figure 9. Relative frequency of the FINCH-INP sizes measured with the APS over the whole campaign period (dashed line) in comparison to the relative frequency of ambient aerosol particle sizes measured with an OPS (solid line).

10616

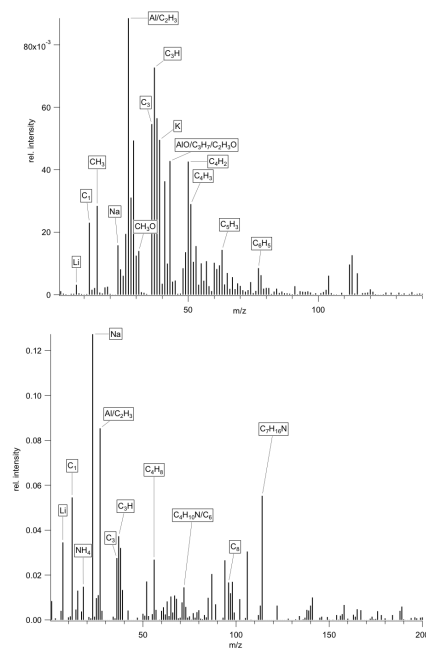


Figure 10. Examples for INP mass spectra measured online with the single particle mass spectrometer ALABAMA behind the FINCH + IN-PCVI. Both particle spectra are dominated by organic ions, but elements like Li and Al might also indicate that these particles may be mineral dust coated with organic matter.